

# Zero-shot Reconstruction of In-Scene Object Manipulation from Video

Dixuan Lin<sup>\*1</sup>, Tianyou Wang<sup>\*2</sup>, Zhuoyang Pan<sup>1</sup>, Yufu Wang<sup>†1</sup>, Lingjie Liu<sup>1</sup>, and Kostas Daniilidis<sup>1</sup>

<sup>1</sup>University of Pennsylvania    <sup>2</sup>University of Oxford

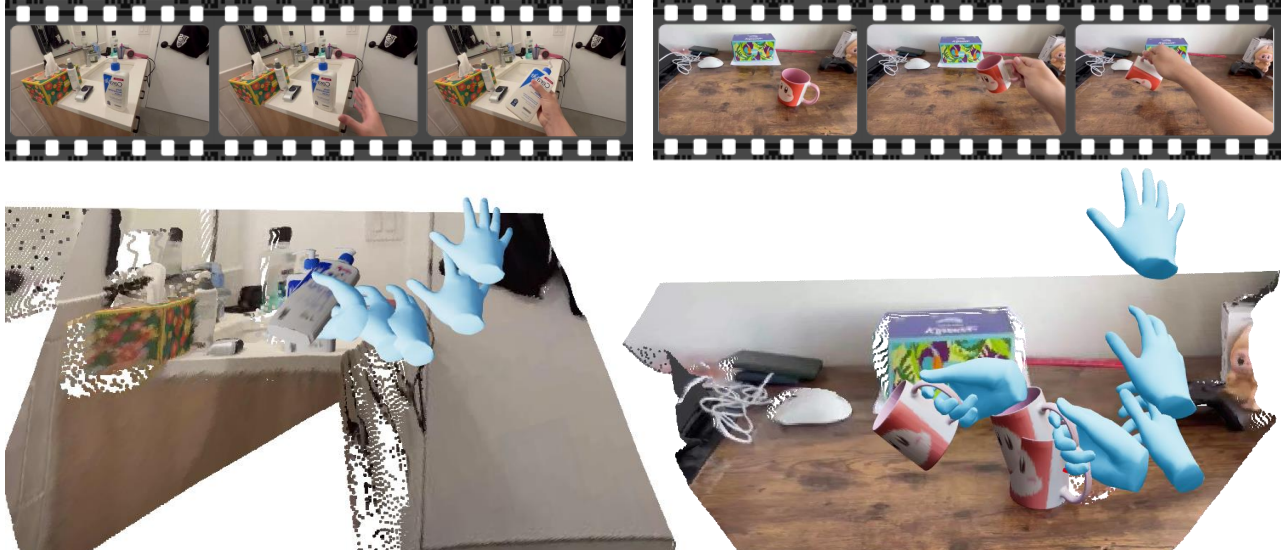


Figure 1. We present a zero shot system that reconstruct in-scene object manipulation motion from daily videos.

## Abstract

We build the first system to address the problem of reconstructing in-scene object manipulation from a monocular RGB video. It is challenging due to ill-posed scene reconstruction, ambiguous hand-object depth, and the need for physically plausible interactions. Existing methods operate in hand-centric coordinates and ignore the scene, hindering metric accuracy and practical use. In our method, we first use data-driven foundation models to initialize the core components, including the object mesh and poses, the scene point cloud, and the hand poses. We then apply a two-stage optimization that recovers a complete hand-object motion from grasping to interaction, which remains consistent with the scene information observed in the input video. Project Page: [reisom2025.github.io/Reisom.github.io/](https://reisom2025.github.io/Reisom.github.io/).

## 1. Introduction

Reconstructing scene-aligned object manipulation from in-the-wild monocular videos is both practical and impactful.

In policy learning for robots with dexterous hands, a policy must learn not only hand-object interactions, but also how the object is used and how it interacts within the surrounding scene. Likewise, AR/VR applications require consistent alignment among the hand, object, and scene to enable reliable and intuitive control.

However, this problem remains largely unexplored, primarily due to three key challenges: (i) Scene reconstruction from a monocular video is inherently ill-posed. Both classical multi-view geometry pipelines (e.g., COLMAP with MVS[35, 36]) and optimization-based neural scene representations (e.g., NeRF [27], 3D Gaussian splatting[15]) fundamentally require multi-view coverage. (ii) Reconstructing physically plausible grasps and interactions with objects in random shapes remains difficult: methods that perform well on dataset templates often fail to achieve contact-consistent, physically valid interactions in the wild. (iii) Estimating accurate 3D motion of the hand and object within the scene is challenging. Recent hand pose estimation methods [18, 29, 55, 57] achieve high pose accuracy and strong 2D reprojection consistency, but still struggle to predict accurate 3D depth.

Given the above challenges, existing object manipulation reconstruction methods[9, 41, 53] focus only on scene-agnostic interactions, without reconstructing the surrounding scene. Consequently, tasks such as "Placing an apple into the basket on table" or "Lifting a kettle and pouring water into a cup" remain largely unaddressed.

Motivated by this gap, we develop a system that reconstructs object manipulations in scene coordinates. We decompose the problem into sub-tasks and leverage strong specialist models that effectively address each sub-problem to obtain reliable intermediate results. We then obtain a unified final result through an optimization procedure. We address these three main challenges by designing the following components of our system.

**Scene reconstruction.** Recent feed-forward approaches [40] show that data-driven priors alone can produce strong reconstructions, preserving accurate geometry without hand-crafted constraints and generalizing to previously unseen objects and scenes. We leverage priors from scene reconstruction methods to generate a scene point cloud from a single monocular view.

**Hand-object interaction.** We first obtain realistic object meshes utilizing the power of learning-based mesh recovery methods [22, 45, 48] which learned strong priors from large 3D asset corpora. Subsequently, we employ a 2D-to-3D contact point matching algorithm to identify corresponding contact points on hand and object, and optimize the motion to obtain a physically plausible hand-object interaction.

**Motion detection and recovery.** The hand's high degrees of freedom and deformability make metric depth estimation via 2D-3D correspondence fundamentally unreliable. In contrast, shifting the focus to the object greatly simplifies the problem. Using object reconstruction methods, we obtain a textured 3D shape that we model as a rigid body; this enables robust 2D feature matching and recovery of its 6-DoF pose trajectory. Once the object's pose is localized in the scene, we use it as an anchor to align the hand trajectory, yielding a consistent, scene-aligned motion.

The main contributions of this work are as follows: We introduce the first system that reconstructs scene-aligned hand-object manipulation from monocular RGB video. We demonstrate robust performance on standard benchmarks as well as in-the-wild videos.

## 2. Related Works

### 2.1. Hand Pose Estimation

Recovering accurate 3D hand pose underpins understanding of human actions and interactions, and has enabled downstream applications such as robotic manipulation[4, 16, 17, 37, 38]. Given the ease of acquiring RGB data and the need for scalable deployment in real-world applications, there has been growing work on estimating 3D hand pose

from an RGB image[13, 19, 21, 28-31, 34, 57, 61, 62] or monocular video[7, 14, 20, 47, 55, 58]. Image-based methods focus on per-frame reconstruction, enforcing consistency with observations, and improving robustness under occlusion. The representative work is HaMeR[29], which scales the training data and adopts a large ViT backbone to achieve strong performance on in-the-wild images. However, these approaches predict hand poses in a canonical space, and depth along the viewing direction is unconstrained, introducing ambiguity and scale mismatch; this limits accuracy and deployment for downstream usability. Our method adopts HaMeR for grasping-frame hand initialization and performs a subsequent optimization to enforce metric-correct depth along each sequence. Video-based methods leverage temporal continuity to enforce coherent and stable 3D hand pose trajectories across frames. Recent work Dyn-HaMR[58] presents an optimization-based pipeline, which integrates camera motion estimation and a learned interaction prior to recover 4D hand motion with a moving camera and interacting hands. Another paradigm, HaPTIC[55] and OmniHands[20] are feed-forward methods. They extend HaMeR to process multiple frames jointly with cross-view self-attention and global cross-attention, and predict metric depth change to output coherent 4D hand trajectories. As HaPTIC showed promising performance in global trajectory accuracy, our system uses it to initialize the entire sequences, except the grasping frame, before optimizing for metric depths and hand-object interaction.

### 2.2. Hand-Object Pose Estimation

Hand-object pose estimation goes beyond hand-only modeling by additionally recovering object pose and shape, and enforcing physically plausible hand-object interactions. Prior work spans several directions. Template-based pipelines[1, 8, 11, 23, 39, 49, 50, 60, 63] often assume a known object template, then estimate 6D object and human pose, e.g., HUMAN[11] fits pose with reprojection and contact terms given the ground truth 3D CAD models. However, template-based pipelines hinge on object model availability thus are hard to scale in the wild. On the other hand, template-free methods utilize multi-view cues or data-driven priors to reconstruct unseen objects from RGB videos[9, 12, 41, 43, 53, 54] or an RGB image[5, 6, 52, 59]. DiffHOI[53] leverages both by optimizing an object SDF and hand mesh over a video with multi-view reprojection from original views and a diffusion prior. DiffHOI requires category level hand-object supervision, while HOLD[9] is a category-agnostic pipeline that jointly reconstructs hands and unknown objects from a single monocular video by training a compositional implicit SDF model that disentangles hand/object geometry and uses contact/mask cues for pose refinement. However, these work require per-sequence test-time fitting, which is time

consuming and prevents a single model across diverse objects, scenes, and actions. MCC-HO[43] presents a complementary retrieval-augmented feed-forward paradigm that infers a hand-conditioned object from RGB image, then retrieves a plausible 3D object via a text-to-3D generative model and rigidly aligns it over time, yielding temporally consistent trajectories for the hand-held object. Despite progress, these template-free pipelines often leave the non-holding sections unaddressed, which makes it hard to handle long-horizon manipulation. Across the directions, the surrounding scene is not constructed, and they often operate in hand-coordinates, which limits global depth/scale reasoning and downstream deployment. Our proposed system reconstructs a metrically aligned scene, uses a strong mesh prior for realistic object geometry, and optimizes a scene-aligned hand-object motion over the entire sequence, including non-holding and holding stages, while bridging gaps from detection failures via a human motion prior.

### 3. Method

#### 3.1. Problem formulation

Given an RGB video  $\mathbf{V} \in \mathbb{R}^{T \times H \times W \times 3}$  of human manipulating an object, our goal is to reconstruct the scene, textured object mesh and hand-object motion in the scene. We represent scene geometry as a colored point cloud  $\mathcal{P}$ . The object  $\Omega = (\mathcal{V}_o, \mathcal{F}_o)$  is modeled as a textured mesh with vertices  $\mathcal{V}_o$  and faces  $\mathcal{F}_o$ . Object trajectories are parameterized by 6d poses  $\mathcal{O} \in \mathbb{R}^{T \times 6}$ . For hand representation, we adopt the MANO parametric model[33], which includes subject-specific shape parameters  $\beta \in \mathbb{R}^{10}$  and time-varying pose  $\theta \in \mathbb{R}^{T \times 48}$  and global translation  $\tau \in \mathbb{R}^{T \times 3}$ . We denote the hand parameters as  $\mathcal{H} = (\theta, \beta, \tau)$ . We first describe how to reconstruct core elements as initialization using existing priors in Section 3.2, then explain how our optimization integrates these elements into a consistent 3D world in Section 3.3.

#### 3.2. Initial Reconstructions

For the scene and object components, we follow OnePoseviaGen[10] to reconstruct the scene, the object in the scene, and the object’s 6D pose trajectory. For hand pose, we adopt HaPTIC[55] as the baseline to extract the hand trajectory. We now describe each component in detail.

Before all the components, we first run SAM2[32] on the entire video to get the consistent masks of the object.

**Scene Reconstruction.** We reconstruct the scene by running SpatialTrackerV2[46] to estimate video-consistent depth maps together with camera intrinsics and extrinsics. A pixel  $(u, v)$  with depth  $D_t(u, v)$  is back-projected to a 3D world point using the pinhole model (with world-to-camera extrinsics  $[\mathbf{R}_t | \mathbf{t}_t]$  and intrinsics  $\mathbf{K}$ ):

$$P_t = \left\{ \mathbf{R}_t^\top (D_t(u, v) \mathbf{K}^{-1} [u, v, 1]^\top - \mathbf{t}_t) \mid (u, v) \in \Omega \right\},$$

where  $\Omega$  denotes the set of valid pixels. Aggregating points over all  $(u, v) \in \Omega$  for each frame  $t$  forms a per-frame point cloud; concatenating across frames yields a dense, globally aligned scene reconstruction.

**Textured Object Reconstruction.** For textured object reconstruction, we send the first frame of the masked object image of the sequence to the State-of-the-art Image-to-3D generators. We route non-occluded objects to Hi3DGen[51] and occluded objects to Amodal3R[44].

**Object Pose Reconstruction.** Given the image depth, camera intrinsics, and the generated object model, we further query Foundationpose[42] to get the 6D object pose for each frames. We improve original Oneposeviagen by registering once on the first frame then tracking through the entire video, instead of querying 6D poses frame by frame.

**Hand Pose Reconstruction.** For the full-video hand reconstruction, we adopt HaPTIC[55] as the backbone to produce sequences with coherent dynamics and smooth pose  $\hat{\theta}$  and transitions  $\hat{\tau}$ . We perform a subsequent optimization to recover metric-accurate depths consistent with the RGB evidence, yielding scene-aligned hand trajectories.

#### 3.3. Hand-Object Motion Optimization

##### 3.3.1. Two Stage Splitting

We decompose the hand-object motion into two stages: grasping and interaction. The grasping stage spans from the hand’s approach to the onset of grasp. The interaction stage begins at grasp and covers the subsequent manipulation. This decomposition offers three benefits.

(i) Objective disentanglement. In grasping, we target smooth, penetration-free translation. In interaction, we prioritize stable contact and object-conditioned motion. Jointly optimizing both introduces conflicting goals. (ii) Results from interaction optimization can be feedback to resolve the depth ambiguity that often remains in the grasping stage. (iii) Sequential extensibility. The two-stage design naturally handles multi-object sequences: approach (Stage 1), interact (Stage 2), then repeat Stage 1 for the next object.

We infer the grasping frame by the estimated object pose  $\mathcal{O} = \{(o_0, r_0), \dots, (o_T, r_T)\}$ , where  $o_i$  represents the object center translation at frame  $i$  and  $r_i$  represents the orientation. We set a translational threshold  $\epsilon_o$  and a rotational threshold  $\epsilon_r$ . If, starting at time  $t^*$ , the changes exceed these thresholds for  $m$  consecutive frames, we regard  $t^*$  as the grasping frame. Let  $\Delta o_k$  and  $\Delta r_k$  denote the changes in position and rotation, the computation is given below:

$$t_o^* = \inf \left\{ t \geq m : \min_{k \in \{t-m+1, \dots, t\}} \|\Delta o_k\|_2 > \epsilon_o \right\} \quad (1)$$

$$t_r^* = \inf \left\{ t \geq m : \min_{k \in \{t-m+1, \dots, t\}} \|\Delta r_k\|_2 > \epsilon_r \right\} \quad (2)$$

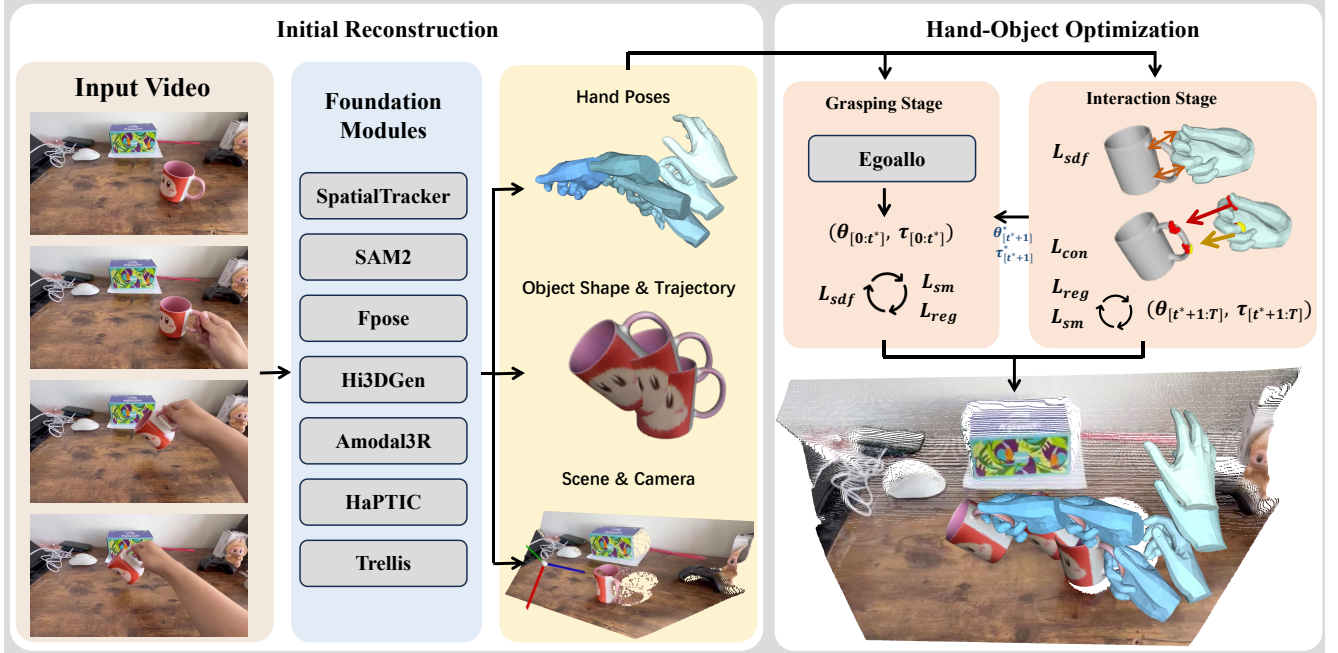


Figure 2. Overview of our framework. We first use foundation models to obtain the hand pose, object, and scene (Sec 3.2). We then optimize hand–object interaction in the interaction stage by computing contact points and enforcing physical collision constraints (Sec 3.3.2). Finally, in the grasping optimization stage, we complete the motion using a human motion prior and further optimize the approaching and grasping phases (Sec 3.3.3).

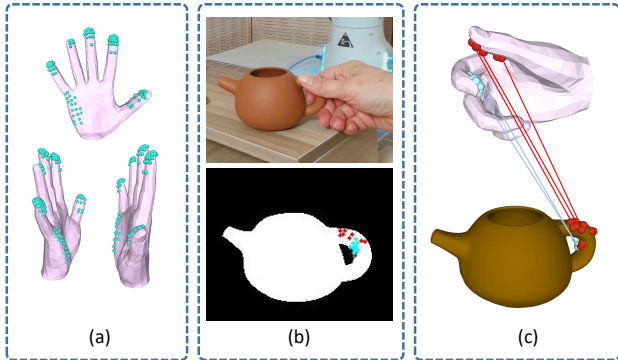


Figure 3. (a) Contact candidates. (b) Top: input image. Bottom: the 2D projections of the contact candidates and their intersections with the object mask, where sky blue denotes back-surface contacts and red denotes front-surface contacts. (c) The correspondence between hand and object contact points.

Then we obtain  $t^* = \min(t_o^*, t_r^*)$ . We estimate the stationary pose of the object by averaging its pose in frames preceding grasping.

$$\hat{\mathcal{O}}_{[0:t^*]} = \frac{1}{t^* + 1} \sum_{i=0}^{t^*} \mathcal{O}_i \quad (3)$$

For the object poses after grasping, we leverage One-

Euro Filter[2] to obtain a smoother trajectory  $\hat{\mathcal{O}}_{[t^*+1:T]}$ . The detailed procedures are in the supplementary material.

### 3.3.2. Interaction Stage Optimization

During optimization, we first optimize the interaction stage to obtain a depth-consistent hand–object motion, then use the resulting depth estimates to optimize the grasping stage. In this stage, our goal is to find optimal hand poses  $\theta^*$  and translations  $\tau^*$  by several constraints:

$$(\theta^*, \tau^*) = \inf_{(\theta, \tau)} \{ \lambda_1 L_{con} + \lambda_2 L_{sdf} + \lambda_3 L_{sm} + \lambda_4 L_{reg} \} \quad (4)$$

Next, we detail the semantics of these constraints.

**Constraints on contact Points.** To align the hand and object in 3D, we match corresponding contact points. In prior work[25, 41], sampling contact candidates from hand vertices is a choice shown to be efficient and effective. As demonstrated in Figure 3, we sample 115 contact candidates  $\mathcal{V}_c$  distributed in fingertips and treat these as potential contacts, shown in (a). Based on the intuition that vertices in contact in 3D also coincide in 2D, we project the candidate points onto the image plane using the camera intrinsics  $K_s$  to obtain 2D contact candidates  $\mathcal{U}_c = \Pi_{K_s}(\mathcal{V}_c)$ .

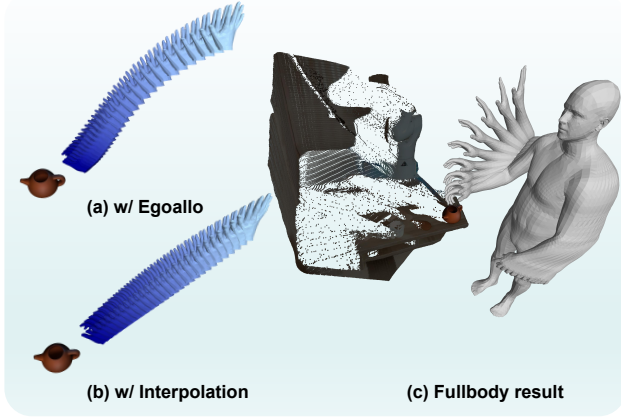


Figure 4. Comparison of Egoallo generated motion, interpolation and fullbody motion. The initial hand pose is set to a half-raised posture. Darker color indicates progression over time. (a) shows the hand motion trajectory obtained with EgoAllo. (b) shows the trajectory produced by interpolation. (c) shows the full-body motion trajectory recovered by EgoAllo.

With object mesh  $\Omega$  and object pose  $\hat{O}$ , we render a mask  $M$  under the same camera intrinsics. Consequently, we compute the intersections of 2D contact candidates and object mask, which serve as the 2d contact points:

$$\mathcal{U}_\phi = M \cap \mathcal{U}_c \quad (5)$$

We proceed by pairing the 2D points with their 3D matches. Each 2D contact point corresponds to a hand vertex and a surface point on the object mesh. For hand-side contacts, we directly map the 2D contact set  $\mathcal{U}_\phi$  to the corresponding 3D hand vertices  $\mathcal{V}_\phi$  via their vertex indices. To find an object-side contact, we cast a ray from the camera through the 2D pixel, the contact lies at the intersection of this ray with the object surface. For a watertight object, the ray intersects the surface an even number of times, so we must decide whether the contact occurs on the front or back surface.

Using MANO[33], we obtain per-vertex normals  $\mathcal{N}_h$  on the posed hand. Thus, for each 2D index, the corresponding hand-vertex normal is  $\mathcal{N}_\phi$ . With the viewing direction defined as the positive z-axis, vertices whose normal satisfies  $z > 0$  face away from the camera and are classified as back-surface hand contacts  $\mathcal{V}_b$ , whereas vertices whose normal satisfies  $z < 0$  face toward the camera and are classified as front-surface hand contacts  $\mathcal{V}_f$ . For  $\mathcal{V}_f$ , their corresponding contact points on the object  $O_f$  lie in the first intersections of the rays on the object surface. For  $\mathcal{V}_b$ , their contact points on the object  $O_b$  are in the last intersections. Then we define the contact loss as a distance loss:

$$L_{\text{con}} = \frac{1}{|\mathcal{V}_b|} \sum_{i=1}^{|\mathcal{V}_b|} \left\| \mathbf{v}_b^{(i)} - \mathbf{o}_b^{(i)} \right\|_2 + \frac{1}{|\mathcal{V}_f|} \sum_{i=1}^{|\mathcal{V}_f|} \left\| \mathbf{v}_f^{(i)} - \mathbf{o}_f^{(i)} \right\|_2 \quad (6)$$

**Constraints on Penetration.** Achieving a physically plausible grasp requires preventing finger–object interpenetration. We enforce a hand–object collision constraint using an SDF loss. Specifically, given a watertight object, we compute its signed distance field and denote the signed distance of hand vertex  $v_i$  to the object surface by  $d(v_i)$ . The distance is positive when the vertex is outside the surface, and negative if inside. The penetration loss can be computed by:

$$L_{\text{sdf}} = \sum_{v \in \mathcal{V}_h} d(v) \quad (7)$$

where  $\mathcal{V}_h$  refers to hand vertices.

**Constraints on Motion Smoothness.** Since hand pose and position should evolve smoothly throughout the motion, we enforce a smoothness loss. Specifically, we regularize temporal changes in the hand pose  $\theta$  and the trajectories of the fingertip joints  $\mathcal{J}^{tip}$ :

$$L_{\text{sm}} = \frac{1}{T - t^* - 2} \sum_{t=t^*+1}^{T-1} (\|\Delta\theta_{[t]}\| + \frac{1}{|\mathcal{J}^{tip}|} \sum_{j \in \mathcal{J}^{tip}} \|\Delta j_{[t]}\|) \quad (8)$$

where  $\Delta\theta_{[t]}$  is the rotational change from frame  $t$  to  $t + 1$  and  $\Delta j_{[t]}$  refers to the change in joint position.

**Constraints on Regularization.** We aim to optimize physical contact while preserving the original hand pose as much as possible, so we add a regularization term that penalizes deviations from the foundation model’s pose, which imposes a larger penalty as the optimized pose drifts farther from this reference:

$$L_{\text{reg}} = \frac{1}{T - t^* - 1} \|\hat{\theta}_{[t^*+1:T]} - \theta_{[t^*+1:T]}\| \quad (9)$$

where  $\hat{\theta}$  denotes the pose estimated by the hand-detection baseline.

### 3.3.3. Grasping Stage Optimization

**Grasp frame alignment.** In this stage, we take the hand motion sequence  $(\hat{\theta}_{[0:t^*]}, \hat{\tau}_{[0:t^*]}, \hat{\beta})$  extracted from Section 3.2 as the initialization. After optimization of the interaction stage, we have already aligned the hand position in scene coordinate at the end of the grasping stage. Therefore, we initialize the target position  $\hat{\tau}_{[t^*]}$  for the grasping stage using the optimized  $\tau_{[t^*+1]}^*$  from the interaction stage.

$$\hat{\tau}_{[0:t^*]} \leftarrow \hat{\tau}_{[0:t^*]} - \hat{\tau}_{[t^*]} + \tau_{[t^*+1]}^* \quad (10)$$

**Motion completion via human motion prior.** During the approaching stage, the hand often moves from outside the camera’s field of view into the visible region. Since

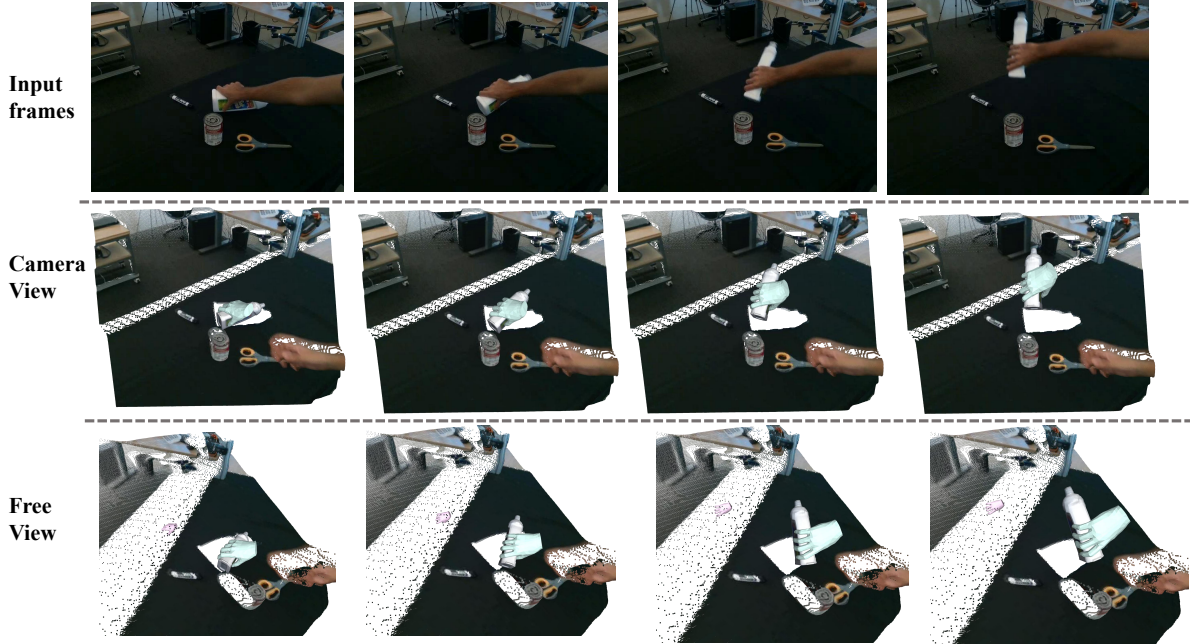


Figure 5. Qualitative results on DexYCB. We visualize our reconstruction of the scene and object in 2 views, with the hand mesh shown in blue. In free view, the baseline hand reconstruction is overlaid in pink for comparison.

our hand detection algorithm is only effective in the hand visible frames  $\mathcal{I}$ , only initial pose and translation in these frames  $\{\hat{\theta}_{[i]}, \hat{\tau}_{[i]}\}_{i \in \mathcal{I}}$  are reliable, which requires us to complete the full hand motion. For the unseen segments outside the field of view, we aim to generate a complete approaching motion starting from a given initial pose. We require this motion to be smooth, kinematically plausible, and consistent with the valid poses at visible frames. To this end, we use Egoallo [56], a human motion prior to complete the motion using the guidance we have:

$$(\tilde{\theta}, \tilde{\tau}) = \pi(\{\hat{\theta}_{[i]}, \hat{\tau}_{[i]}\}_{i \in \mathcal{I}}) \quad (11)$$

By this prior, we achieve a complete approaching trajectory. In Figure 4, we compare the motion trajectories generated by the guided motion prior with those obtained by interpolation and with real human motion. A thorough analysis of the effectiveness of this motion prior is provided in Section 4.4.

**Grasping motion optimization.** We then use  $(\tilde{\theta}, \tilde{\tau})$  as the initialization for the subsequent optimization. Our goal in this stage is to smoothen the approaching and grasping motion as well as avoiding finger-object interpenetration. We utilize smoothness loss to make the grasp pose coincide with the first frame of the second stage and further regularize the entire motion to be smoother. To prevent mesh interpenetration, we also impose an SDF loss as a constraint. The overall optimization loss for this phase can be represented:

$$L_{grasp} = \lambda_5 L_{sdf} + \lambda_6 L_{sm} + \lambda_7 L_{reg} \quad (12)$$

By optimizing with respect to the above constraints, we obtain  $(\theta^*_{[0:t^*]}, \tau^*_{[0:t^*]})$ . We discuss the details of the parameter settings in the supplementary material.

## 4. Experiments

To validate the effectiveness of our method, we evaluate it on two widely used hand-object datasets: DexYCB [3] and HOI4D [24]. Since no existing methods address in-scene object manipulation, we compare our approach against our baseline and its global-aligned version.

### 4.1. Datasets

**DexYCB**[3] consists of videos in which 20 distinct YCB objects are grasped by hand, captured from 10 different viewpoints. Since our method is template-free, to reconstruct the object we filter out sequences where the target object is occluded by other objects retaining only those where it remains continuously visible and unobstructed. From this subset, we sampled 120 sequences, with an average of 52.11 frames per sequence.

**HOI4D**[24] is a hand-object interaction video dataset captured with head-mounted cameras, containing both rigid and articulated objects. We evaluate on the rigid subset: “ToyCar,” “Mug,” “Bottle,” “Bowl,” “Kettle,” and “Knife.” We split each action segment within a video into a separate sequence. Similarly, we sampled 120 sequences from both the training and test splits for evaluation, with an average of 133.52 frames per sequence.



Figure 6. Qualitative results on in-the-wild videos. We evaluate on videos involving everyday object manipulation, including translating objects to target locations and rotating object orientations. We present results across multiple viewpoints and time instants, and compare them against the baseline.

Table 1. Quantitative evaluation for in-scene object manipulation. We evaluate on two widely used HOI datasets HOI4D and DexYCB. We compare with the hand motion reconstruction baseline HaPTIC and the version it aligns the ground-truth wrist. We highlight the best values in bold.

Dataset	Method	MPJPE ↓	MRPE ↓	IV-mean ↓	IV-max ↓	ID-mean ↓	ID-max ↓	JM ↓
HOI4D	HaPTIC[55]	19.15	137.63	-	-	-	-	<b>1.50</b>
	HaPTIC <sup>†</sup>	<b>19.15</b>	-	3.53	10.15	10.22	29.31	3.22
	Ours	20.48	<b>64.10</b>	<b>0.46</b>	<b>4.34</b>	<b>3.68</b>	<b>24.24</b>	2.38
DexYCB	HaPTIC	7.88	150.72	-	-	-	-	0.82
	HaPTIC <sup>†</sup>	7.88	-	8.91	14.25	15.14	35.69	<b>0.71</b>
	Ours	<b>7.67</b>	<b>45.71</b>	<b>0.14</b>	<b>0.98</b>	<b>7.72</b>	<b>35.45</b>	1.96

## 4.2. Evaluation Metrics

We evaluate both reconstruction accuracy and physical plausibility. Pose accuracy is measured by Mean Per Joint Position Error (MPJPE), and motion accuracy by Mean Root Position Error (MRPE), defined as the mean distance between predicted and ground-truth wrist positions over the sequence after aligning the first frame. Hand-object contact is assessed using interpenetration Volume (IV) and interpenetration Depth (ID), for which we report mean and maximum values, and motion smoothness is quantified by jerk magnitude (JM). MPJPE and MRPE are computed only on frames where the hand is visible, while IV, ID, and JM are computed over all frames in the interaction stage.

## 4.3. Comparison Results

**Quantitative Results.** We primarily compare hand pose accuracy, trajectory deviation, and a suite of physics-based metrics for hand-object interaction on DexYCB[3] and HOI4D[24]. Since there are currently no other hand-object

interaction methods operating in the world coordinate frame, we compare against baseline approach HaPTIC, which reconstructs hand motion in world coordinate frame. The detailed results are presented in Table 1. Since HaPTIC does not reconstruct objects, physical metrics cannot be computed directly. To enable a more informative comparison, we report HaPTIC<sup>†</sup>, obtained by aligning each frame’s hand wrist to the ground-truth wrist position, and then computing the physical metrics between reconstructed hand and the ground-truth object.

From the table, we observe that HaPTIC reconstructs reasonably accurate hand poses, but depth ambiguity leads to large trajectory errors. The HaPTIC<sup>†</sup> results further show that even after aligning the wrist to the ground truth, uncertainty in object shape yields substantial physical errors in the grasp configuration. In our method, reconstructing the object’s 3D shape enables more faithful recovery of the hand grasp. On HOI4D, because the ground truth itself contains hand-object penetrations, enforcing our physical optimization slightly degrades MPJPE.

Table 2. We ablate our components on DexYCB relative to the base model, reporting MPJPE, MRPE, and physics-based measures under different loss configurations. Row 1 is the unoptimized baseline, row 2 adds a contact loss with translation-only optimization, and rows 3–7 jointly optimize translation and pose with progressively richer loss combinations.

$L_{con}$	$L_{sdf}$	$L_{reg}$	$L_{sm}$	MPJPE ↓	MRPE ↓	IV-mean ↓	IV-max ↓	ID-mean ↓	ID-max ↓	JM ↓
×	×	×	×	7.88	150.72	-	-	-	-	0.82
✓	×	×	×	7.88	53.91	5.57	7.13	13.42	36.12	0.99
×	✓	✓	✓	7.83	149.67	<b>0.01</b>	<b>0.07</b>	<b>0.36</b>	<b>2.50</b>	<b>0.67</b>
✓	×	✓	✓	7.52	43.98	6.71	8.15	14.83	39.75	1.36
✓	✓	×	✓	27.04	50.11	0.19	1.07	5.14	30.77	1.51
✓	✓	✓	×	<b>7.49</b>	<b>40.92</b>	0.08	0.74	5.20	28.93	9.53
✓	✓	✓	✓	7.67	45.71	0.14	0.98	7.72	35.45	1.96

Table 3. We report the discrepancy between the motions generated by Egoallo and their corresponding guidance.

Dataset	MPJPE	G-MRPE
DexYCB[3]	0.041	0.170
HOI4D[24]	0.087	0.134

**Qualitative Results.** We present qualitative results in Figure 5 and Figure 6 on DexYCB and in-the-wild videos, respectively, visualizing the reconstructed scene, object, and hand motion. For each example, we show the input video frame, the reconstruction from the camera view, and a second free-view rendering. We also demonstrate comparisons with our baseline. The results indicate that our method produces correct grasps and accurate world-coordinate hand–object motion trajectories, whereas the baseline, due to depth ambiguity, fails to interact properly with the object.

#### 4.4. Ablation Studies.

##### Effectiveness of optimization components.

We conduct an ablation study on the optimization components using DexYCB. Table 2 reports results under different combinations of constraints.

Since our alignment hinges on contact points, omitting the contact loss yields little to no hand–object contact, which in turn produces deceptively low interpenetration metrics. In row 2 we Enable the contact loss while optimizing translation only. The results already delivers a notable boost in trajectory accuracy, underscoring the value of contact constraints. Removing the SDF loss eliminates collision penalties: pose and trajectory errors decrease, but both penetration volume and depth increase markedly. The fifth row illustrates the role of the regularization restriction, without it, optimization drifts toward physically plausible poses while deviating from the input observations. Finally, ablating the smoothness term can improve per-frame accuracy, but it introduces pronounced jitter over the full sequence. In the last row, using all constraints yields the best overall performance.

##### Effectiveness of human motion prior.

We employ the human motion prior EgoAllo [56] to complete the approaching trajectory in Section 3.3.3. EgoAllo is a diffusion-based human motion prior that can generate smooth motion, allowing control over hand movements via guidance signals. We provide discrete hand poses and wrist positions as guidance to generate the entire motion sequence. Figure 4 compares trajectories produced with the motion prior versus interpolation. Our known inputs include the hand’s positions and poses on visible frames and a prescribed initial pose. As shown in (a), EgoAllo yields a trajectory that follows plausible human kinematics, whereas (b) the interpolated result exhibits mechanically linear motion. In (c), we visualize EgoAllo’s full-body output, which further demonstrates the realism and consistency of the completed motion.

We quantitatively compare the input guidance to the corresponding generated outputs: MPJPE evaluates pose deviation, and global MRPE measures trajectory deviation. As shown in Table 4, the MPJPE error is less than 0.1 mm, indicating that, in practice, the guidance and the generated results are effectively identical.

## 5. Discussion

**Limitations and future work.** Our method relies on the accuracy of scene segmentation and the subsequent object reconstruction. In low-light conditions or under severe motion blur, object reconstruction may fail, which in turn prevents us from identifying correct contact points in the interaction stage. In addition, we currently perform object reconstruction using only the first frame, whereas in principle we could exploit object observations from the entire video, which is a promising direction for future improvement.

**Conclusion.** We presented the first system for in-scene object manipulation reconstruction. We jointly estimate the whole scene and object-hand motion in scene frame coordinate, obtain the approaching motion and the interaction motion separately through a two-stage optimization scheme, and achieve strong performance on in-the-wild videos.

## References

- [1] Bharat Lal Bhatnagar, Xianghui Xie, Ilya A Petrov, Cristian Sminchisescu, Christian Theobalt, and Gerard Pons-Moll. Behave: Dataset and method for tracking human object interactions. In *Proceedings of the IEEE/CVF Conference on Computer Vision and Pattern Recognition*, pages 15935–15946, 2022. 2
- [2] Géry Casiez, Nicolas Roussel, and Daniel Vogel. 1€ filter: a simple speed-based low-pass filter for noisy input in interactive systems. In *Proceedings of the SIGCHI Conference on Human Factors in Computing Systems*, pages 2527–2530, 2012. 4, 1
- [3] Yu-Wei Chao, Wei Yang, Yu Xiang, Pavlo Molchanov, Ankur Handa, Jonathan Tremblay, Yashraj S Narang, Karl Van Wyk, Umar Iqbal, Stan Birchfield, et al. Dexycb: A benchmark for capturing hand grasping of objects. In *Proceedings of the IEEE/CVF conference on computer vision and pattern recognition*, pages 9044–9053, 2021. 6, 7, 8
- [4] Guangyan Chen, Meiling Wang, Te Cui, Yao Mu, Haoyang Lu, Tianxing Zhou, Zicai Peng, Mengxiao Hu, Haizhou Li, Li Yuan, et al. Vlmimic: Vision language models are visual imitation learner for fine-grained actions. *Advances in Neural Information Processing Systems*, 37:77860–77887, 2024. 2
- [5] Zerui Chen, Yana Hasson, Cordelia Schmid, and Ivan Laptev. Alignsdf: Pose-aligned signed distance fields for hand-object reconstruction. In *European conference on computer vision*, pages 231–248. Springer, 2022. 2
- [6] Zerui Chen, Shizhe Chen, Cordelia Schmid, and Ivan Laptev. gsdf: Geometry-driven signed distance functions for 3d hand-object reconstruction. In *Proceedings of the IEEE/CVF conference on computer vision and pattern recognition*, pages 12890–12900, 2023. 2
- [7] Enes Duran, Muhammed Kocabas, Vasileios Choutas, Zicong Fan, and Michael J Black. Hmp: Hand motion priors for pose and shape estimation from video. In *Proceedings of the IEEE/CVF Winter Conference on Applications of Computer Vision*, pages 6353–6363, 2024. 2
- [8] Zicong Fan, Omid Taheri, Dimitrios Tzionas, Muhammed Kocabas, Manuel Kaufmann, Michael J Black, and Otmar Hilliges. Arctic: A dataset for dexterous bimanual hand-object manipulation. In *Proceedings of the IEEE/CVF conference on computer vision and pattern recognition*, pages 12943–12954, 2023. 2
- [9] Zicong Fan, Maria Parelli, Maria Eleni Kadoglou, Xu Chen, Muhammed Kocabas, Michael J Black, and Otmar Hilliges. Hold: Category-agnostic 3d reconstruction of interacting hands and objects from video. In *Proceedings of the IEEE/CVF Conference on Computer Vision and Pattern Recognition*, pages 494–504, 2024. 2
- [10] Zheng Geng, Nan Wang, Shaocong Xu, Chongjie Ye, Bohan Li, Zhaoxi Chen, Sida Peng, and Hao Zhao. One view, many worlds: Single-image to 3d object meets generative domain randomization for one-shot 6d pose estimation. *arXiv preprint arXiv:2509.07978*, 2025. 3
- [11] Yana Hasson, Gül Varol, Cordelia Schmid, and Ivan Laptev. Towards unconstrained joint hand-object reconstruction from rgb videos. In *2021 International Conference on 3D Vision (3DV)*, pages 659–668. IEEE, 2021. 2
- [12] Di Huang, Xiaopeng Ji, Xingyi He, Jiaming Sun, Tong He, Qing Shuai, Wanli Ouyang, and Xiaowei Zhou. Reconstructing hand-held objects from monocular video. In *SIGGRAPH Asia 2022 Conference Papers*, pages 1–9, 2022. 2
- [13] Zheheng Jiang, Hossein Rahmani, Sue Black, and Bryan M Williams. A probabilistic attention model with occlusion-aware texture regression for 3d hand reconstruction from a single rgb image. In *Proceedings of the IEEE/CVF conference on computer vision and pattern recognition*, pages 758–767, 2023. 2
- [14] Korrawe Karunratanakul, Sergey Prokudin, Otmar Hilliges, and Siyu Tang. Harp: Personalized hand reconstruction from a monocular rgb video. In *Proceedings of the IEEE/CVF conference on computer vision and pattern recognition*, pages 12802–12813, 2023. 2
- [15] Bernhard Kerbl, Georgios Kopanas, Thomas Leimkühler, and George Drettakis. 3d gaussian splatting for real-time radiance field rendering. *ACM Trans. Graph.*, 42(4):139–1, 2023. 1
- [16] Justin Kerr, Chung Min Kim, Mingxuan Wu, Brent Yi, Qianqian Wang, Ken Goldberg, and Angjoo Kanazawa. Robot see robot do: Imitating articulated object manipulation with monocular 4d reconstruction. *arXiv preprint arXiv:2409.18121*, 2024. 2
- [17] Jinhan Li, Yifeng Zhu, Yuqi Xie, Zhenyu Jiang, Mingyo Seo, Georgios Pavlakos, and Yuke Zhu. Okami: Teaching humanoid robots manipulation skills through single video imitation. *arXiv preprint arXiv:2410.11792*, 2024. 2
- [18] Mengcheng Li, Liang An, Hongwen Zhang, Lianpeng Wu, Feng Chen, Tao Yu, and Yebin Liu. Interacting attention graph for single image two-hand reconstruction. In *Proceedings of the IEEE/CVF conference on computer vision and pattern recognition*, pages 2761–2770, 2022. 1
- [19] Mengcheng Li, Hongwen Zhang, Yuxiang Zhang, Ruizhi Shao, Tao Yu, and Yebin Liu. Hhmr: Holistic hand mesh recovery by enhancing the multimodal controllability of graph diffusion models. In *Proceedings of the IEEE/CVF Conference on Computer Vision and Pattern Recognition*, pages 645–654, 2024. 2
- [20] Dixuan Lin, Yuxiang Zhang, Mengcheng Li, Yebin Liu, Wei Jing, Qi Yan, Qianying Wang, and Hongwen Zhang. Omni-hands: Towards robust 4d hand mesh recovery via a versatile transformer. *arXiv preprint arXiv:2405.20330*, 2024. 2
- [21] Kevin Lin, Lijuan Wang, and Zicheng Liu. Mesh graphormer. In *Proceedings of the IEEE/CVF international conference on computer vision*, pages 12939–12948, 2021. 2
- [22] Minghua Liu, Chong Zeng, Xinyue Wei, Ruoxi Shi, Linghao Chen, Chao Xu, Mengqi Zhang, Zhaoning Wang, Xiaoshuai Zhang, Isabella Liu, et al. Meshformer: High-quality mesh generation with 3d-guided reconstruction model. *Advances in Neural Information Processing Systems*, 37:59314–59341, 2024. 2
- [23] Shaowei Liu, Hanwen Jiang, Jiarui Xu, Sifei Liu, and Xiaolong Wang. Semi-supervised 3d hand-object poses estimation with interactions in time. In *Proceedings of*

- the *IEEE/CVF conference on computer vision and pattern recognition*, pages 14687–14697, 2021. 2
- [24] Yunze Liu, Yun Liu, Che Jiang, Kangbo Lyu, Weikang Wan, Hao Shen, Boqiang Liang, Zhoujie Fu, He Wang, and Li Yi. Hoi4d: A 4d egocentric dataset for category-level human-object interaction. In *Proceedings of the IEEE/CVF Conference on Computer Vision and Pattern Recognition*, pages 21013–21022, 2022. 6, 7, 8
- [25] Yumeng Liu, Xiaoxiao Long, Zemin Yang, Yuan Liu, Marc Habermann, Christian Theobalt, Yuexin Ma, and Wenping Wang. Easyhoi: Unleashing the power of large models for reconstructing hand-object interactions in the wild. In *Proceedings of the Computer Vision and Pattern Recognition Conference*, pages 7037–7047, 2025. 4
- [26] Matthew Loper, Naureen Mahmood, Javier Romero, Gerard Pons-Moll, and Michael J Black. Smpl: A skinned multi-person linear model. In *Seminal Graphics Papers: Pushing the Boundaries, Volume 2*, pages 851–866. 2023. 1
- [27] Ben Mildenhall, Pratul P Srinivasan, Matthew Tancik, Jonathan T Barron, Ravi Ramamoorthi, and Ren Ng. Nerf: Representing scenes as neural radiance fields for view synthesis. *Communications of the ACM*, 65(1):99–106, 2021. 1
- [28] JoonKyu Park, Yeonguk Oh, Gyeongsik Moon, Hongsuk Choi, and Kyoung Mu Lee. Handocnet: Occlusion-robust 3d hand mesh estimation network. In *Proceedings of the IEEE/CVF conference on computer vision and pattern recognition*, pages 1496–1505, 2022. 2
- [29] Georgios Pavlakos, Dandan Shan, Ilija Radosavovic, Angjoo Kanazawa, David Fouhey, and Jitendra Malik. Reconstructing hands in 3d with transformers. In *Proceedings of the IEEE/CVF Conference on Computer Vision and Pattern Recognition*, pages 9826–9836, 2024. 1, 2
- [30] Rolandos Alexandros Potamias, Jinglei Zhang, Jiankang Deng, and Stefanos Zafeiriou. Wilor: End-to-end 3d hand localization and reconstruction in-the-wild. In *Proceedings of the Computer Vision and Pattern Recognition Conference*, pages 12242–12254, 2025.
- [31] Aditya Prakash, Ruisen Tu, Matthew Chang, and Saurabh Gupta. 3d hand pose estimation in everyday egocentric images. In *European Conference on Computer Vision*, pages 183–202. Springer, 2024. 2
- [32] Nikhila Ravi, Valentin Gabeur, Yuan-Ting Hu, Ronghang Hu, Chaitanya Ryali, Tengyu Ma, Haitham Khedr, Roman Rädle, Chloe Rolland, Laura Gustafson, et al. Sam 2: Segment anything in images and videos. *arXiv preprint arXiv:2408.00714*, 2024. 3
- [33] Javier Romero, Dimitrios Tzionas, and Michael J Black. Embodied hands: Modeling and capturing hands and bodies together. *arXiv preprint arXiv:2201.02610*, 2022. 3, 5, 1
- [34] Yu Rong, Takaaki Shiratori, and Hanbyul Joo. Frankmocap: A monocular 3d whole-body pose estimation system via regression and integration. In *Proceedings of the IEEE/CVF International Conference on Computer Vision*, pages 1749–1759, 2021. 2
- [35] Johannes L Schönberger and Jan-Michael Frahm. Structure-from-motion revisited. In *Proceedings of the IEEE conference on computer vision and pattern recognition*, pages 4104–4113, 2016. 1
- [36] Johannes L Schönberger, Enliang Zheng, Jan-Michael Frahm, and Marc Pollefeys. Pixelwise view selection for unstructured multi-view stereo. In *European conference on computer vision*, pages 501–518. Springer, 2016. 1
- [37] Junyao Shi, Zhuolun Zhao, Tianyou Wang, Ian Pedroza, Amy Luo, Jie Wang, Jason Ma, and Dinesh Jayaraman. Zeromimic: Distilling robotic manipulation skills from web videos. *arXiv preprint arXiv:2503.23877*, 2025. 2
- [38] Himanshu Gaurav Singh, Antonio Loquercio, Carmelo Sferazza, Jane Wu, Haozhi Qi, Pieter Abbeel, and Jitendra Malik. Hand-object interaction pretraining from videos. In *2025 IEEE International Conference on Robotics and Automation (ICRA)*, pages 3352–3360. IEEE, 2025. 2
- [39] Bugra Tekin, Federica Bogo, and Marc Pollefeys. H+o: Unified egocentric recognition of 3d hand-object poses and interactions. In *Proceedings of the IEEE/CVF conference on computer vision and pattern recognition*, pages 4511–4520, 2019. 2
- [40] Jianyuan Wang, Minghao Chen, Nikita Karaev, Andrea Vedaldi, Christian Rupprecht, and David Novotny. Vggt: Visual geometry grounded transformer. In *Proceedings of the Computer Vision and Pattern Recognition Conference*, pages 5294–5306, 2025. 2
- [41] Shibo Wang, Haonan He, Maria Pirelli, Christoph Gebhardt, Zicong Fan, and Jie Song. Magichoi: Leveraging 3d priors for accurate hand-object reconstruction from short monocular video clips. In *Proceedings of the IEEE/CVF International Conference on Computer Vision*, pages 5957–5968, 2025. 2, 4
- [42] Bowen Wen, Wei Yang, Jan Kautz, and Stan Birchfield. Foundationpose: Unified 6d pose estimation and tracking of novel objects. In *Proceedings of the IEEE/CVF Conference on Computer Vision and Pattern Recognition*, pages 17868–17879, 2024. 3
- [43] Jane Wu, Georgios Pavlakos, Georgia Gkioxari, and Jitendra Malik. Reconstructing hand-held objects in 3d from images and videos. *arXiv preprint arXiv:2404.06507*, 2024. 2, 3
- [44] Tianhao Wu, Chuanxia Zheng, Frank Guan, Andrea Vedaldi, and Tat-Jen Cham. Amodal3r: Amodal 3d reconstruction from occluded 2d images. *arXiv preprint arXiv:2503.13439*, 2025. 3
- [45] Jianfeng Xiang, Zelong Lv, Sicheng Xu, Yu Deng, Ruicheng Wang, Bowen Zhang, Dong Chen, Xin Tong, and Jiaolong Yang. Structured 3d latents for scalable and versatile 3d generation. In *Proceedings of the Computer Vision and Pattern Recognition Conference*, pages 21469–21480, 2025. 2
- [46] Yuxi Xiao, Jianyuan Wang, Nan Xue, Nikita Karaev, Yuri Makarov, Bingyi Kang, Xing Zhu, Hujun Bao, Yujun Shen, and Xiaowei Zhou. Spatialtrackerv2: 3d point tracking made easy. *arXiv preprint arXiv:2507.12462*, 2025. 3, 1
- [47] Hao Xu, Tianyu Wang, Xiao Tang, and Chi-Wing Fu. H2onet: Hand-occlusion-and-orientation-aware network for real-time 3d hand mesh reconstruction. In *Proceedings of the IEEE/CVF conference on computer vision and pattern recognition*, pages 17048–17058, 2023. 2

- [48] Jiale Xu, Weihao Cheng, Yiming Gao, Xintao Wang, Shenghua Gao, and Ying Shan. Instantmesh: Efficient 3d mesh generation from a single image with sparse-view large reconstruction models. *arXiv preprint arXiv:2404.07191*, 2024. [2](#)
- [49] Lixin Yang, Xinyu Zhan, Kailin Li, Wenqiang Xu, Jiefeng Li, and Cewu Lu. Cpf: Learning a contact potential field to model the hand-object interaction. In *Proceedings of the IEEE/CVF international conference on computer vision*, pages 11097–11106, 2021. [2](#)
- [50] Lixin Yang, Kailin Li, Xinyu Zhan, Jun Lv, Wenqiang Xu, Jiefeng Li, and Cewu Lu. Artiboost: Boosting articulated 3d hand-object pose estimation via online exploration and synthesis. In *Proceedings of the IEEE/CVF conference on computer vision and pattern recognition*, pages 2750–2760, 2022. [2](#)
- [51] Chongjie Ye, Yushuang Wu, Ziteng Lu, Jiahao Chang, Xiaoyang Guo, Jiaqing Zhou, Hao Zhao, and Xiaoguang Han. Hi3dgen: High-fidelity 3d geometry generation from images via normal bridging. *arXiv preprint arXiv:2503.22236*, 3:2, 2025. [3](#)
- [52] Yufei Ye, Abhinav Gupta, and Shubham Tulsiani. What’s in your hands? 3d reconstruction of generic objects in hands. In *Proceedings of the IEEE/CVF conference on computer vision and pattern recognition*, pages 3895–3905, 2022. [2](#)
- [53] Yufei Ye, Poorvi Hebbbar, Abhinav Gupta, and Shubham Tulsiani. Diffusion-guided reconstruction of everyday hand-object interaction clips. In *Proceedings of the IEEE/CVF international conference on computer vision*, pages 19717–19728, 2023. [2](#)
- [54] Yufei Ye, Abhinav Gupta, Kris Kitani, and Shubham Tulsiani. G-hop: Generative hand-object prior for interaction reconstruction and grasp synthesis. In *Proceedings of the IEEE/CVF Conference on Computer Vision and Pattern Recognition*, pages 1911–1920, 2024. [2](#)
- [55] Yufei Ye, Yao Feng, Omid Taheri, Haiwen Feng, Shubham Tulsiani, and Michael J Black. Predicting 4d hand trajectory from monocular videos. *arXiv preprint arXiv:2501.08329*, 2025. [1](#), [2](#), [3](#), [7](#)
- [56] Brent Yi, Vickie Ye, Maya Zheng, Yunqi Li, Lea Müller, Georgios Pavlakos, Yi Ma, Jitendra Malik, and Angjoo Kanazawa. Estimating body and hand motion in an ego-sensed world. In *Proceedings of the Computer Vision and Pattern Recognition Conference*, pages 7072–7084, 2025. [6](#), [8](#), [1](#)
- [57] Zhengdi Yu, Shaoli Huang, Chen Fang, Toby P Breckon, and Jue Wang. Acr: Attention collaboration-based regressor for arbitrary two-hand reconstruction. In *Proceedings of the IEEE/CVF conference on computer vision and pattern recognition*, pages 12955–12964, 2023. [1](#), [2](#)
- [58] Zhengdi Yu, Stefanos Zafeiriou, and Tolga Birdal. Dynamr: Recovering 4d interacting hand motion from a dynamic camera. In *Proceedings of the Computer Vision and Pattern Recognition Conference*, pages 27716–27726, 2025. [2](#)
- [59] Chenyangguang Zhang, Guanlong Jiao, Yan Di, Gu Wang, Ziqin Huang, Ruida Zhang, Fabian Manhardt, Bowen Fu, Federico Tombari, and Xiangyang Ji. Moho: Learning single-view hand-held object reconstruction with multi-view occlusion-aware supervision. In *Proceedings of the IEEE/CVF Conference on Computer Vision and Pattern Recognition*, pages 9992–10002, 2024. [2](#)
- [60] Jason Y Zhang, Sam Pepose, Hanbyul Joo, Deva Ramanan, Jitendra Malik, and Angjoo Kanazawa. Perceiving 3d human-object spatial arrangements from a single image in the wild. In *European conference on computer vision*, pages 34–51. Springer, 2020. [2](#)
- [61] Xiong Zhang, Qiang Li, Hong Mo, Wenbo Zhang, and Wen Zheng. End-to-end hand mesh recovery from a monocular rgb image. In *Proceedings of the IEEE/CVF international conference on computer vision*, pages 2354–2364, 2019. [2](#)
- [62] Zhishan Zhou, Shihao Zhou, Zhi Lv, Mingqiang Zou, Yao Tang, and Jiajun Liang. A simple baseline for efficient hand mesh reconstruction. In *Proceedings of the IEEE/CVF Conference on Computer Vision and Pattern Recognition*, pages 1367–1376, 2024. [2](#)
- [63] Zhifan Zhu and Dima Damen. Get a grip: Reconstructing hand-object stable grasps in egocentric videos. *arXiv preprint arXiv:2312.15719*, 2023. [2](#)

# Zero-shot Reconstruction of In-Scene Object Manipulation from Video

## Supplementary Material

### A. Parameter Setting

We run our method on an NVIDIA L40 GPU. In Grasping stage optimization, we optimize 2000 steps with the learning rate  $10^{-2}$ . In Interaction optimization, we optimize 8000 steps with the learning rate  $5 \times 10^{-3}$ . The loss weights we set in our method are as follow:  $\lambda_1 = 2, \lambda_2 = 5, \lambda_3 = 1, \lambda_4 = 5, \lambda_5 = 2, \lambda_6 = 1, \lambda_7 = 5$ . The units of our metrics are: MPJPE(mm), MRPE(mm), IV( $cm^3$ ), ID(mm), JM( $mm/s^3$ ).

### B. Object pose processing

For object poses in grasping stage, we estimate the stationary pose by averaging its pose in frames preceding grasping:

$$\hat{\mathcal{O}}_{[0:t^*]} = \frac{1}{t^* + 1} \sum_{i=0}^{t^*} \mathcal{O}_i \quad (13)$$

For the interaction stage, we apply a One-Euro filter[2] to smooth the motion sequence. We set the minimum cutoff frequency to  $f_{\min} = 1.5$ , the derivative cutoff frequency to  $f_d = 1.0$ , the speed coefficient to  $\beta = 0.01$ , and the sampling interval to  $\Delta t = 15$ . We define the smoothing factor as:

$$\alpha(f, \Delta t) = \frac{\Delta t}{\Delta t + \frac{1}{2\pi f}} \quad (14)$$

Initializaiton:

$$\hat{o}_{t^*} = o_{t^*}, \quad \hat{g}_{t^*} = \mathbf{0} \quad (15)$$

For each  $t^* < k < T$ , we first estimate the derivative:

$$g_k = \frac{o_k - \hat{o}_{k-1}}{\Delta t_k} \quad (16)$$

Then low-pass filter the derivative:

$$\hat{o}_k = \alpha(f_d, \Delta t_k) g_k + (1 - \alpha(f_d, \Delta t_k)) \hat{g}_{k-1} \quad (17)$$

Compute the adaptive main cutoff frequency:

$$f_c^{(k)} = f_{\min} + \beta \|\hat{g}_k\|_2 \quad (18)$$

Finally output the update:

$$\hat{o}_k = \alpha(f_c^{(k)}, \Delta t_k) o_k + (1 - \alpha(f_c^{(k)}, \Delta t_k)) \hat{o}_{k-1}. \quad (19)$$

After applying the above filtering, we obtain  $\hat{\mathcal{O}}_{[t^*+1:T]}$ .

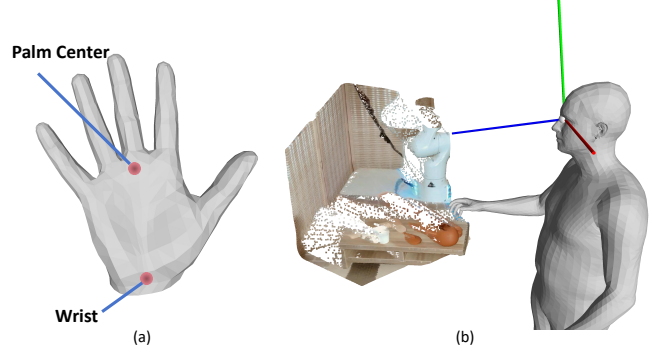


Figure 7. We show (a) Positions of palm center and wrist on hand. (b) Input CPF coordinate and the corresponding generated SMPL-H human mesh.

### C. Application of Egoallo

Egoallo[56] takes a sequence of central pupil frame (CPF) as input and outputs a sequence of human motion represented by SMPL-H[26, 33], which aligns with the CPF.

We initialize the CPF using the camera pose  $[\mathbf{R}_t | \mathbf{t}_t]$  predicted by SpatialTrackerV2[46], which roughly corresponds to a human viewing the object. However, since the manipulating hand is not always aligned with the camera's egocentric viewpoint, we further adjust the CPF orientation and position according to the hand direction, ensuring that the resulting input corresponds to a natural human pose.

Our world coordinate system is defined as an object-centered frame with the  $z$ -axis pointing upward. To obtain a natural body pose and position, we align the CPF orientation with the grasping hand. Specifically, we use the MANO [33] "Palm Center" and "Wrist" joints as anchors (Figure 7(a)) and cast a ray from the wrist to the palm center. We project this ray onto the  $xy$ -plane and compute its azimuth angle  $r_{\text{hand}}$  around the  $z$ -axis. Similarly, we project the CPF viewing direction which is its local  $z$ -axis onto the  $xy$ -plane in the world frame and obtain  $r_{\text{cpf}}$ . We then compute the angular difference

$$\Delta r = \min(r_{\text{hand}} - r_{\text{cpf}}, \frac{\pi}{6}) \quad (20)$$

We expect that the hand-pointing direction does not deviate too much from the viewing direction (at most  $30^\circ$ ). When this angular difference exceeds  $30^\circ$ , we rotate the CPF around the  $z$ -axis in the world coordinate system, centered at the object, by  $\Delta r$ . Figure 7(b) shows the CPF after this adjustment, together with the resulting human body pose and position.